ACS OMEGA

Open Access

This article is licensed under CC-BY-NC-ND 4.0

http://pubs.acs.org/journal/acsodf

Article

Ultrafast and Reproducible Synthesis of Tailor-Made Octacalcium Phosphate

Rajan Choudhary,* Abhishek Indurkar, Kristaps Rubenis, Andra Grava, Arita Dubnika, Katrin Hurle, and Janis Locs*

Cite This: *ACS Omega* 2024, 9, 36165−36176

Read Online

ACCESS | Metrics & More | Article Recommendations | Supporting Information

ABSTRACT: Octacalcium phosphate (OCP) has excellent bone formation ability and a good resorption rate as compared to the commercial bone substitutes [*e.g.*, Bio-Oss (Geistlich Pharma AG) and MBCP+ (Biomatlante)], as well as synthesized biomaterials (hydroxyapatite and tricalcium phosphate). The synthesis approach to obtain phase-pure OCP possesses a great challenge due to its complex reaction mechanism and narrow synthesis window. Thus, the current study aimed to overcome the synthesis challenges and to define the precise reaction conditions required for controllable and reproducible synthesis of OCP. Using the principles of the coprecipitation method, novel synthesis protocols were developed ensuring ultrafast synthesis of OCP within minutes. XRD analysis confirmed that phase-pure OCP was obtained. These processing schemes enabled the synthesis of tailor-made OCP with specific surface areas ranging from 16 to 91 m^2/g. The synthesized OCPs exhibited plate-like morphology. The interaction of the synthesized OCPs with MC3T3-E1 cells was found to be nontoxic, confirming their cytocompatibility. The synthesis approach developed in this study indicates that challenges such as the reaction volume, stirring rate, and flow rate need to be addressed in the future to upscale the technology.

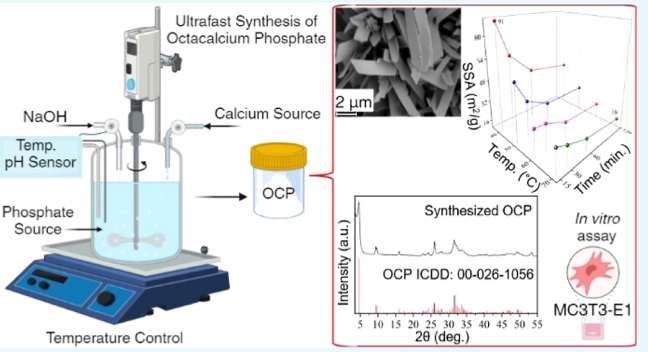

1. INTRODUCTION

Octacalcium phosphate (OCP) [$Ca_8H_2(PO_4)_6{\cdot}5H_2O$, Ca/P ratio: 1.33] is recognized as a precursor of biological apatite crystals in hard tissues.[1] The structure of OCP is composed of an apatitic layer and a hydrated layer stacked alternatively to each other.[2] The atomic arrangements of Ca^{2+} and PO_4^{3-} ions in the apatite layers of the OCP structure are identical to those found in the hydroxyapatite structure.[3] Initially, a two-dimensional nucleus of OCP with a thickness of one unit cell is formed, which grows subsequently into carbonated apatite.[4,5] Natural occurrence of OCP was reported in calcifying dentine and urinary calculus.[6] Even though studies suggest OCP as a precursor of bioapatite, these theories still remain controversial due to the complex biomineralization process.[7]

OCP is recommended as a substitute for autogenic bone grafts due to its intrinsic property to stimulate bone formation.[8,9] Synthetic OCP has shown excellent bone formation ability and a good resorption rate as compared to commercial bone substitutes in various animal studies.[10−12] OCP promoted bone tissue formation within 1 week after being implanted in mouse calvaria defect, whereas dicalcium phosphate and amorphous calcium phosphate (CaP) (3 weeks) and hydroxyapatite (HAp) (5 weeks) revealed delayed tissue appearance.[1] The *in vivo* study performed by Suzuki and his colleagues reported enhanced bone formation on the surface of OCP with higher alkaline phosphatase activity in comparison to HAp.[13] Moreover, OCP has potential to initiate osteoblast differentiation without using any inductive media and is suggested as an osteoinductive material for restoring bone defects.[14,15] Although OCP seems to have been widely investigated, the synthesis approach to obtain phase-pure OCP still possesses a significant challenge. The narrow opportunity window to obtain OCP, complex synthesis, and proper control over its phase purity has limited its valorization and clinical applications.[2] The sole commercial OCP-containing product "Bontree" (Hudens Bio) available on the market is a mixture of OCP and HAp phases.[12]

Precipitation and hydrolysis are the most common methods employed for the synthesis of OCP. The synthesis of OCP is governed by the common ion effect, Gibbs free energy, molarity, pH, temperature, mixing order, and stirring rate.[16,17] A minor modification in these reaction parameters often leads

Received: February 14, 2024
Revised: July 27, 2024
Accepted: July 30, 2024
Published: August 14, 2024

© 2024 The Authors. Published by American Chemical Society

to the formation of brushite or hydroxyapatite, that compromises the purity of OCP. To date, numerous attempts have been made for the synthesis of OCP, but the current methodologies are found to be time-consuming and involving multistep procedures, so that the entire reaction process can take days to complete.[18] Most of the published scientific studies lack precise data (Table 1) for the synthesis of OCP.

Table 1. Overview of OCP Synthesis Conditions Reported in the Literature[a]

S. no	temperature (°C)	pH	time	Ca/P ratio
1	60	5−6	3 to 4 h[19]	1
	70 and 80	4 to 4.5	1 h[19]	1
2	67.5	NA	1 h[20]	1
3	50, 60, and 70	NA	3, 6, and 12 h[21]	1.33
	60	NA	3 h[21]	1.33
4	25	NA	113 h[22]	NA
	45	4.5	12 h[22]	NA
5	60	5	NA[23,24]	NA
6	60	5	50 min, 3 h aging[25,26]	1.33
7	70	5	NA[27]	1.33
8	45−55	6.49−7.17	2 days[14]	NA
9	80	NA	2 h[28]	NA
10	60	NA	3 h[29]	NA
11	80	NA	24 h[30]	NA
12	70	6	2 days[31]	NA
13	70	9	2 days[32]	NA
14	80	6.81	1 day[33]	NA
15	37	4 to 8.8	NA[34]	NA
16	35	NA	24 h[35]	NA

[a]NA: information not available.

The objective of the present work was to develop a precise, controllable, and reproducible procedure for the synthesis of OCP. The influence of reaction pH, order of reagent addition, temperature, and time on phase formation of OCP was investigated. For the first time, detailed optimization of reaction parameters assisting in the synthesis of tailor-made OCP with different surface areas is presented. Moreover, the cytocompatibility of the OCP sample [highest and lowest specific surface area (SSA)] was also evaluated.

2. EXPERIMENTAL SECTION

2.1. Materials and Methods. Calcium acetate hydrate (Merck, 99%), sodium hydroxide (Merck, 99%), sodium dihydrogen phosphate dihydrate (Merck, 99%), and distilled water were used as the starting chemicals. All chemicals were used as received from the manufacturer. The reaction was performed using the synthesis workstation Easy Max 402 reactor (Mettler Toledo). The Easy Max reactor was equipped with a pH sensor, temperature probe, overhead stirrer, and dosing unit SP300 for pH adjustment. Titronic (SI Analytics) was used as the dosing equipment.

OCP was synthesized by the coprecipitation method. Stock solutions of calcium acetate hydrate (0.0532 M), sodium dihydrogen phosphate dihydrate (0.04 M), and sodium hydroxide (3 M) were prepared in deionized water. The calcium and phosphate stock solutions used in this experiment had molar concentrations equivalent to a Ca/P ratio of 1.33 (which corresponds to the Ca/P ratio in the OCP). The calcium acetate solution was filled in the Duran-capped bottle connected to the Titronic dosing equipment, whereas the sodium hydroxide solution bottle was attached to the dosing unit SP 300 of the reactor. Later, 200 mL of sodium dihydrogen phosphate dihydrate solution was transferred to the 400 mL glass vessel kept in the reactor. This reaction vessel was closed by using a glass lid. The pH sensor, temperature probe, overhead stirrer, and dosing unit outlets were mounted in the reaction vessel *via* flanges.

The phosphate source was heated to 40 °C with constant stirring. After attaining the desired temperature, the calcium source (200 mL) was added dropwise to the phosphate source for 15 min. Initially, the influence of different pH values (5.5 to 6.5) on the precipitation of the OCP was studied. Additionally, experiments were conducted in which the pH was not controlled. The equipment was programmed to maintain the desired pH of the reaction mixture by automatically adding an appropriate amount of sodium hydroxide. Second, after pH optimization, the reaction was carried out at temperatures ranging from 30 to 70 °C. Similar procedures to the above methodology were performed, but the only difference was in the duration (30, 60, and 120 min) for the addition of calcium solution into phosphate solution. The overall experimental conditions used for the synthesis of OCP are given in Table 2.

Table 2. Optimized Reaction Conditions for the Synthesis of OCP

processing scheme no.	time required for calcium addition (minutes)	temperature (°C)	pH	Ca/P ratio
1	15	40, 50, 60, and 70	6	1.33
2	30			
3	60			
4	120			

After completion, the precipitate was isolated by using vacuum filtration and washed thrice with deionized water. Then, the precipitate was frozen in liquid nitrogen, followed by lyophilization. The synthesis schemes were performed more than ten times to confirm the reproducibility. The influence of different reaction pH, temperature, and time on surface morphology and surface area was studied. Moreover, the effect of the OCP SSA on cytocompatibility was also evaluated.

Additionally, the effect of the order of reagent addition on the formation of the OCP was investigated. In these experiments, the phosphate source was added dropwise to the calcium source for 15 min. The reaction was performed at 40 °C, and the pH was maintained at 6. The filtration and lyophilization steps were performed as mentioned in the above paragraph. XRD analysis of the experiment is discussed in Figure S2.

2.2. Characterization. *2.2.1. OCP Characterization.* Powder XRD (Panalytical, Aeris) was used for phase identification. The XRD instrument operated at 40 kV and 15 mA by utilizing a copper (Cu) tube as its X-ray source. The diffraction data was recorded within the 3−55° 2θ range, employing a 0.04° 2θ step size. The samples were prepared using a backloading sample holder. Each sample underwent 1 h measurement duration. Scanning electron microscopy (SEM, Tescan Mira/LMU) was used to analyze the surface morphology of the synthesized OCP. The powdered sample was fixed on a standard aluminum sample holder with double-sided carbon adhesive carbon tape and then coated with gold using an Emitech K550X system from Quorum Technology.

https://doi.org/10.1021/acsomega.4c01436
ACS Omega 2024, 9, 36165−36176

Attenuated total reflection Fourier transform infrared (FT-IR) spectroscopy (Thermo Fisher) was used to analyze the presence of different functional groups associated with OCP. The FT-IR spectrum was obtained with a resolution of 4 cm^{-1} in the range from 400 to 4000 cm^{-1}. A Brunauer−Emmett−Teller (BET) model was employed to determine SSAs using nitrogen gas adsorption (Quantachrome Instruments). Before conducting the analysis, the OCP samples were subjected to 24 h of vacuum degassing at room temperature.

The particle size distribution of the samples utilized for the *in vitro* cytotoxicity study (40 °C in 15 min and 70 °C in 120 min) was analyzed in dry mode using laser diffraction granulometry (Mastersizer 3000, Malvern Instruments). The median size d0.5 of the OCP samples (equivalent to 50% cumulative volume percentage) was recorded. Particle size analysis was conducted three times for each sample, and the results are presented as the mean value ± the standard deviation.

2.2.2. Powder XRD Analysis and Rietveld Refinement. The OCP powders were characterized with a diffractometer D8 ADVANCE with Da Vinci design (Bruker AXS, Karlsruhe, Germany). The following measurement parameters were applied: range: 2.5−70° 2θ; step size: 0.0112° 2θ; integration time: 1 s; radiation: Cu-K_α; generator settings: 40 kV, 40 mA; divergence slit: variable slit with a fixed sample illumination of 10 mm. The variable divergence slit was chosen to enhance the background in the initial part of the diffraction pattern. The powders were prepared for the measurements by the front loading method; three independently prepared samples of the powders synthesized at 40 and 70 °C for 15 min each were analyzed.

Rietveld analysis of the powders was performed with the software TOPAS V5 (Bruker AXS, Karlsruhe, Germany). The structure model ICSD #65347[36] was used for the refinement of OCP. All lattice parameters of the triclinic structure were refined. The anisotropic crystallite size of OCP was refined with the approach of Ectors *et al.*, (2015),[37] using an elliptic cylinder model. rx was aligned parallel to the crystallographic *b* axis, ry to the *a* axis, and rz to the *c* axis (Figure 1). These three

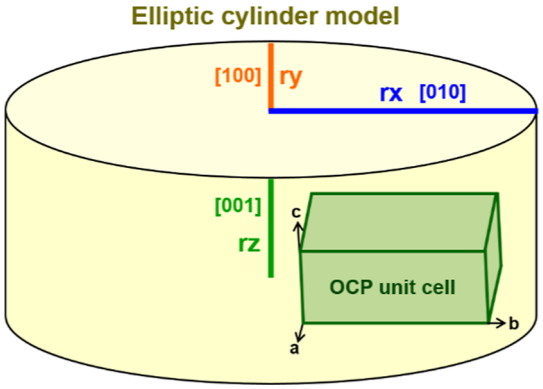

Figure 1. Elliptic cylinder model used for the refinement of anisotropic crystallite sizes in the OCP.

parameters are directly correlated to the OCP crystallite sizes (*i.e.*, the sizes of the coherent scattering domains), in the corresponding crystallographic directions. Microstrain was refined in addition. No preferred orientation was included. A Chebyshev polynomial of the second order was used for the background. Additionally, a *hkl* phase was added to model the elevated background, possibly due to amorphous content present in the sample. A *hkl* phase contains lattice parameters, crystallite size, and space group but no atom positions. Space group $P6_3/m$ (that of hydroxyapatite) was chosen.[38]

2.3. *In Vitro* Cytotoxicity Studies. The OCP samples were sterilized in 70% ethanol for 1 h followed by UV irradiation for 30 min. The cytotoxicity of two types of OCP samples synthesized at 40 and 70 °C (with lowest and highest surface area, see Sections 2.1 and 3.3.4) was tested on the MC3T3-E1 cell line (preosteoblasts). For the extract test, 4500 cells per well were seeded in a 96-well plate in 100 μL of cell medium, which consisted of 89% alpha-modified Eagle medium, supplemented with 10% fetal bovine serum and 1% penicillin/streptomycin (P/S). Phosphate buffered saline (pH 7.4) was added to the wells around the perimeter to prevent the solution on the plate from drying out. Prior to the experiment, the plates with the cells were incubated overnight at 37 °C, with 5% CO_2 (New Brunswick S41i CO_2 Incubator Shaker, Eppendorf, Hamburg, Germany).

Each powder sample was suspended in fresh 5 mL of cell medium obtaining a concentration of 10 mg/mL. After 24 and 48 h, all the solution was collected from the samples and replaced with fresh 5 mL of cell medium. The collected solution was filtrated with a 0.2 μm syringe filter and either used as an undiluted extract or diluted with fresh medium (extract to cell medium 1:10 and 1:100) and immediately put onto the preincubated cells (100 μL for each well). Untreated cells were used as a positive control, while a 5% dimethyl sulfoxide solution in the medium was applied to cells as a negative control. There were six replicates for each treatment.

To assess the cytotoxicity of the OCP extracts and their dilutions, the Cell Counting Kit -8 (CCK-8) assay was used. After 24 h of incubation for each time point, extracts and their dilutions, 10 μL of CCK-8 solution was added to the cultivation media to each well and incubated for 1 h at 37 °C, with 5% CO_2. The absorption at 450 nm was measured using an Infinite M Nano microplate reader (Tecan, Männedorf, Switzerland).

3. RESULTS AND DISCUSSION

3.1. Effect of pH. The pH profiles of all the samples recorded during each experiment and the FT-IR spectra of samples prepared at different pH are provided in the Supporting Information (Figure S1). There were some pH fluctuations but not more than ±0.2. Thus, the precipitation reaction was allowed to occur at the controlled pH. With the change in pH of the reaction mixture, different CaP compounds formed (Figure 2). The precipitation of CaPs occurs spontaneously from supersaturated solutions, followed by a decrease in the pH. The pH of the reaction mixture decreases due to the release of protons. In the current study, when the calcium source was added into the phosphate solution, an increase in pH of the reaction mixture was noticed, and later, a constant decline in the pH level occurred due to the initiation of precipitation reaction. The initial increase in pH was due to the higher pH of the calcium acetate solution as compared with the phosphate solution.

The XRD pattern of the sample prepared without controlling the pH (Figure 2a) revealed that brushite was a dominant phase, whereas when the pH of the reaction mixture was kept at 5.5 (Figure 2b), the sample was found to be composed of two phases corresponding to OCP as well as brushite. When the pH of the reaction mixture was maintained

https://doi.org/10.1021/acsomega.4c01436
ACS Omega 2024, 9, 36165−36176

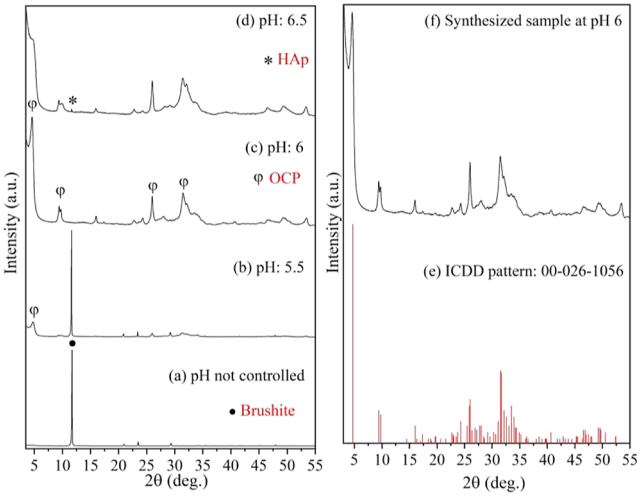

Figure 2. XRD pattern of samples prepared at different pH (a–d) and comparison of the synthesized sample with the ICDD pattern of OCP (e,f).

at 6, the pure OCP phase was obtained (Figure 2c). Furthermore, increasing the pH from 6 to 6.5 resulted in a decrease of the characteristic peak associated with the OCP and the presence of a HAp peak was detected (Figure 2d). This observation revealed that the pH of the reaction can alter the reaction pathway of CaPs and leads to the formation of different CaP phases, even if the reaction mixture contains a constant Ca/P ratio of the desired phase, OCP. The characteristic peaks of the OCP observed in the XRD pattern (Figure 2f) matched with the standard OCP ICDD card no. 00-026-1056 (Figure 2e). This confirmed that the diffraction maxima correspond only to the OCP, and no other phases were identified (Figure 2f). Hence, optimization of the current reaction scheme has established that pH 6 favored the precipitation of OCP.

The potential reason for the formation of different CaP phases is that the variation of pH affects the solubility and changes the equilibrium of phosphate ions in the solution. Decrease of pH results in the shifting of the phosphate ions from PO_4^{3-} (phosphates) to HPO_4^{2-} (hydrogen phosphate) to $H_2PO_4^-$ (dihydrogen phosphate) to H_3PO_4 (phosphoric acid).[39] These ionic variations influence the chemical composition of the end product. Due to this complex equilibrium, it becomes difficult to control the precipitation of the desired product. The dihydrogen phosphate ion ($H_2PO_4^-$) and hydrogen phosphate ion (HPO_4^{2-}) coexist in the investigated pH range (5.5–6) as per the previous study.[21] These ions vary fractionally according to their ionization enthalpy dependent on the reaction temperature as per Van't Hoff's equation.[40] The alteration of the concentration of the required ions and the pH influence the degree of supersaturation (solubility). The reaction mixture becomes oversaturated due to the lower solubility of the OCP, leading to its precipitation. During precipitation, the ionic composition of phosphate species in the reaction mixture is affected by pH. Moreover, it has been reported that the stability of CaPs in an aqueous medium is highly affected by the pH.[41] Previously, Komlev *et al.* employed similar reagents and methodology for the synthesis of OCP.[42] However, their study lacked details on the volume of reagents used, and no description of the pH adjustment was mentioned. The authors observed the formation of brushite and OCP at pH 6 and reported that the brushite formed in the initial stages of the reaction converts to OCP. In the present study, the presence of brushite at pH 6 was not detected.

In the current report, sodium hydroxide (background electrolyte) was used to maintain a constant pH. The ionic strength of sodium hydroxide was 3 M. The ionic strength is associated with the measurement of the concentration of ions in the given solution.[43] The ionic strength of the background electrolyte relates to the presence of ions in the solution, which determines the pH of the reaction mixture and, subsequently, influences the degree of supersaturation. The influence of pH and ionic strength on CaP supersaturation is discussed elsewhere.[44] It was found that at a constant molar concentration of calcium and phosphate ions, the relative supersaturation associated with CaP phases depends on the pH of the reaction mixture. When the ionic concentrations of calcium, phosphate, and hydrogen are kept constant, the degree of supersaturation is dependent on the ionic strength of the solution, which is maintained by the addition of an inert electrolyte (background). It is important to consider that the pH and ionic strength can vary during the precipitation reaction, indicating the complexity of the CaP solution chemistry. Therefore, it is crucial to conduct thermodynamic studies for developing models to predict the formation of CaP phases. Additionally, understanding the reaction kinetics will be more beneficial in predicting the formation of a particular CaP phase under the given conditions. This approach will assist in overcoming the key challenge of understanding the mechanisms of precipitation reactions involving calcium and phosphate ions by calculating the activities of ionic species and the formation of CaP phases during the crystallization process. Thus, additional research is required with a specific focus on the early stages of synthesis to predict the mechanism of the OCP formation.

3.2. Effect of Synthesis Temperature. *3.2.1. XRD and Rietveld Characterization.* The impact of the synthesis temperature on the formation of the OCP at a pH of 6 was studied. The reaction performed at 30 °C indicated the existence of dual phases corresponding to OCP and brushite (Figure 3).

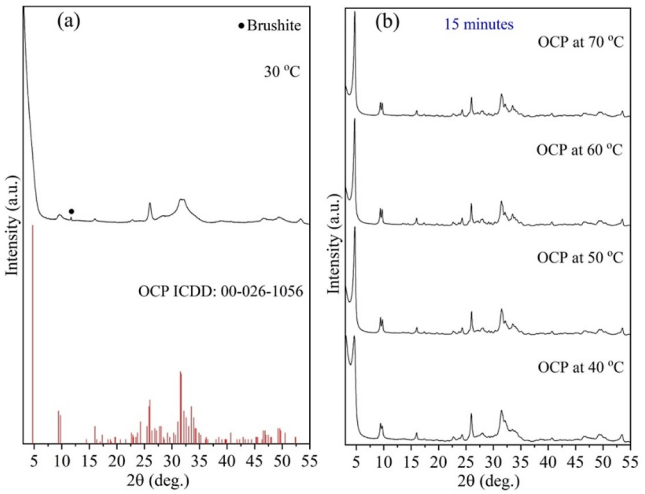

Figure 3. XRD pattern of samples prepared in 15 min at 30 (a) and 40 to 70 °C (b).

https://doi.org/10.1021/acsomega.4c01436
ACS Omega 2024, 9, 36165–36176

The samples prepared at temperatures ranging from 40 to 70 °C reveal the OCP phase. This temperature-specific phase formation response can be associated with the lack of sufficient energy, which acts as a driving force for the precipitation of the OCP. Even though the pH was maintained at 6, the temperature (30 °C) was not enough to propagate the reaction toward the formation of the characteristic OCP phase. Although the OCP characteristic diffraction duplet at 9.4 and 9.7° 2θ can be seen, the main diffraction maxima at 4.7° 2θ cannot be distinguished. Likely, the crystallite size in the [100] direction is very low, resulting in a very broad (100) reflection at around 4.7° 2θ that is hardly visible. Crystallite size in the *b* direction is supposedly higher, thus resulting in more clearly visible (1−10) and (010) reflections between 9 and 10° 2θ.

All peaks observed in the XRD pattern (Figure 3b) matched the standard OCP ICDD card no. 00-026-1056. In addition, all reflections could be fitted in the Rietveld software with structure model ICSD #65347.[36] These findings confirmed that no crystalline secondary phases were present. Moreover, the characteristic (100) reflection of the OCP became higher and sharper with an increase in temperature (Figure 4).

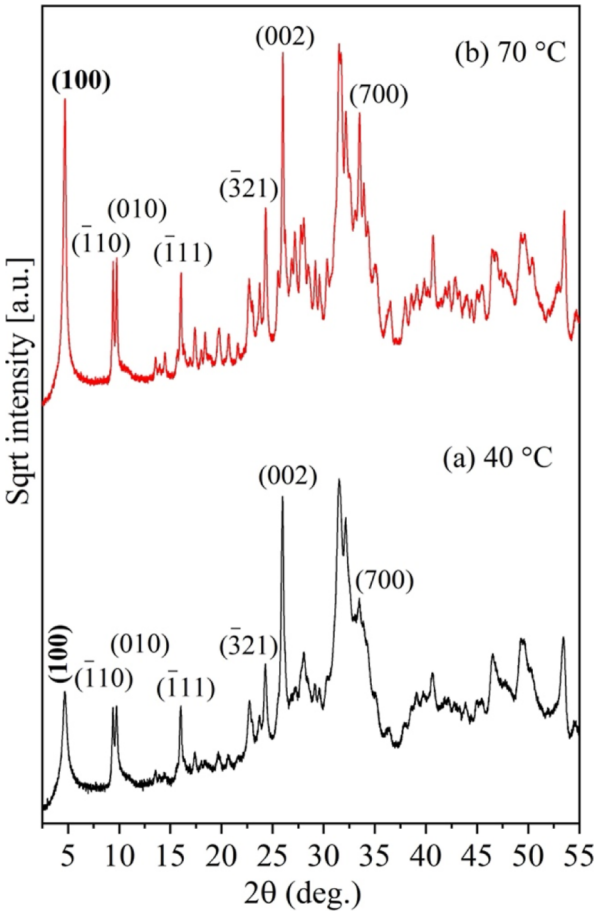

Figure 4. Diffraction patterns of OCP synthesized at 40 (a) and 70 °C (b) for 15 min each.

Accordingly, the radius of the elliptic cylinder model assigned to the [100] direction, correlated to the OCP crystallite size in the [100] direction (*a* axis), increased from 3.2 ± 0.3 nm in the 40 °C sample to 9.9 ± 0.8 nm in the 70 °C sample. No significant change of the radius aligned in [010] direction was observed; it was around 20 nm in both cases.

Previously, the synthesis of OCP was reported in 1 day and 113 h at a temperature of 35 and 25 °C, respectively.[22,35] A recent study utilized a microflow reactor for the synthesis of OCP. The total volume of the synthesis reaction was 36 mL and OCP phase formation was detected only after aging the mother solution at 50 °C for 12 h and at 60 and 70 °C for 3 h, respectively,[21] whereas in the current work, the total reaction volume employed was 11 times more, and the OCP was obtained without any aging step. The methodology developed in the present work is capable of synthesizing OCP within 15 min at temperatures ranging from 40 to 70 °C.

The layered crystal structure of OCP enables the incorporation of carboxylate ions into the hydrated layer.[45] When carboxylate ions are incorporated into the crystal structure of the OCP, this compound is known as OCP carboxylate and commonly abbreviated as OCPC. Rietveld refinement of the a parameter of the OCP crystalline lattice indicated a clear decrease for the 70 °C sample, compared to the 40 °C sample. Due to the inverse correlation between the interplanar distance d and the incident angle θ, as expressed by the Bragg equation $n\cdot\lambda = 2d\cdot\sin\theta$, the corresponding (100) reflection is shifted to a higher °2θ position in the 70 °C sample. Accordingly, decreases were observed for the b and c parameter (Figure 5). The lattice parameters obtained in this

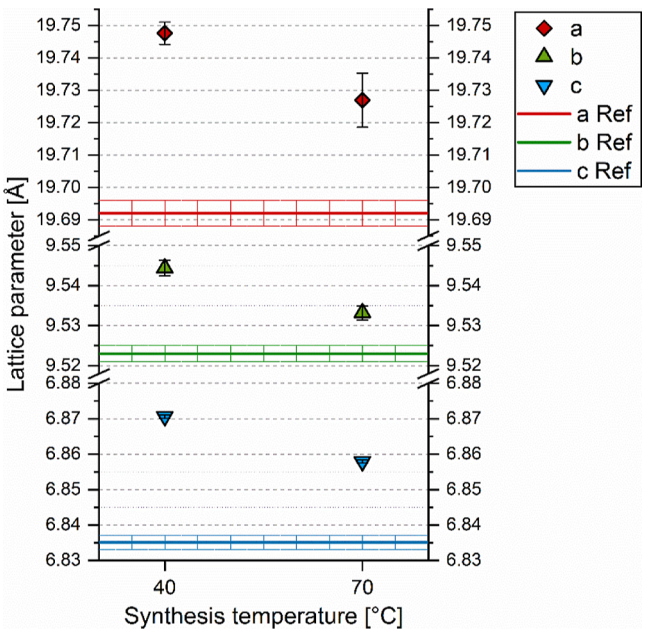

Figure 5. Lattice parameters of OCP synthesized at 40 °C and 70 °C, compared to the lattice parameters provided in the structure model ICSD #65347.[36] The measured data are means of three independent measurements; the error bars represent the standard deviation.

study were further compared with those of the OCP reference structure ICSD #65347.[36] It is evident that for the OCP obtained at 40 and 70 °C, all three measured lattice parameters were significantly higher than those of the standard structure ICSD #65347 (Figure 5). The a parameter of the OCP is not identical to the interplanar spacing (d_{100}) value due to the triclinic symmetry, but d_{100} can be obtained from the a parameters and the angle α from geometric correlations. Accordingly, the d_{100} value of the ICSD 65347 OCP structure is 18.658 Å, whereas the d_{100} value of the 40 °C sample was 18.711 Å. The interplanar spacing d_{100} of 18.658 Å (ICSD

https://doi.org/10.1021/acsomega.4c01436
ACS Omega 2024, 9, 36165−36176

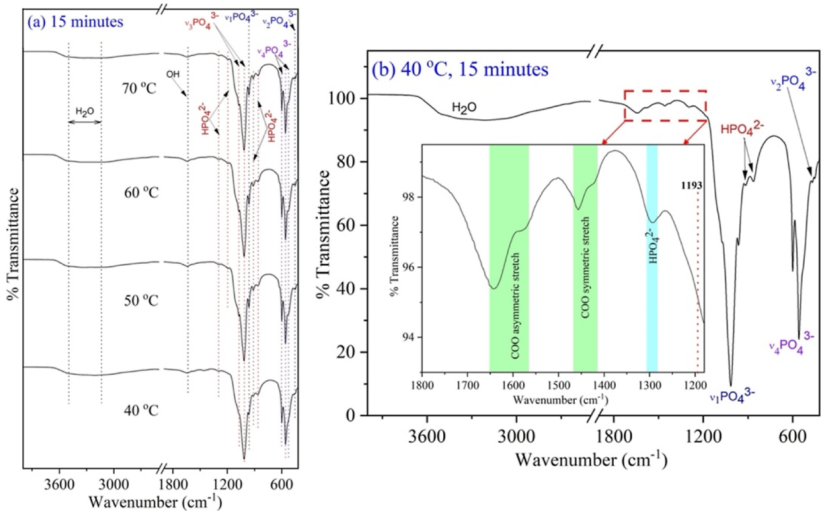

Figure 6. FT-IR spectra of samples prepared in 15 min at different temperatures (a) and at 40 °C (b).

#65347) would correspond to a (100) peak position of 4.732° 2θ for the Cu-K$_\alpha$ radiation used within this study (wavelength: 1.5406 Å), thus differing by 0.013° 2θ from the position of the (100) peak in the 40 °C sample (4.719° 2θ).

The observed increase of lattice parameters, especially the a parameter, of the 40 °C sample compared to the 70 °C sample can be explained by the incorporation of carboxylate ions into OCP, which leads to the shifting of the peak in the XRD pattern and causes variations in the interplanar spacing (d_{100}) of OCP.[45] The incorporation of carboxylate ions in the OCP structure caused the shifting of the (100) refection peak to a lower angle.[45] Previously, it was emphasized that the expansion of the *a* axis indicates the incorporation of carboxylate ions into the crystal plane (100) of OCP.[46] The interplanar spacing values of the present study are lower than those published in reports,[47] as the elongation depends on the number of carbon atoms in the carboxylate ion.[46]

However, it should be noted that carboxylation is not the only possible reason for an increase in the lattice parameters. It is reported that the water content of OCP can be variable.[5] Increase of water content in the hydrate layer would increase d_{100} and hence the a parameter. Therefore, it is possible that only the 40 °C sample is carboxylated, while the increase of the 70 °C sample compared to the reference can be explained by other factors.

3.2.2. FT-IR Analysis. The FT-IR spectra of samples synthesized at different temperatures are shown in Figure 6a. The absorption peaks at 466, 527 to 598 cm^{-1} are associated with the bending vibrations (ν_2, ν_4) of the phosphate group (PO_4^{3-}). The absorption bands at 861, 915, and 1295 cm^{-1} correspond to the stretching vibrations of HPO_4^{2-}, whereas the absorption bands ranging from 961 and 1014 to 1073 cm^{-1} are associated with P−O stretching (ν_1 and ν_3) vibrations.[48] The broad OH stretching vibration was observed at 3400 cm^{-1}, the bending OH vibration was found at 1644 cm^{-1}, and the shoulder peak at 627 cm^{-1} is associated with water.[2] Moreover, the HAp-characteristic OH stretching band at 3572 cm^{-1} was found to be missing, which is a good indicator for the absence of HAp.[49]

This research was focused on developing a protocol for the ultrafast synthesis of the OCP, but surprisingly, we encountered the possible formation of OCPC. FT-IR spectroscopy is an appropriate characterization technique to confirm the incorporation of carboxylate ions into the OCP structure.[45] The absorption band associated with the hydrogen phosphate ions in the hydrated layer of the OCP was noticed at 1193 cm^{-1} in all the samples except the sample prepared at 40 °C (Figure 6b). The disappearance of the absorption peak at 1193 cm^{-1} occurs due to the incorporation of carboxylate ions in the OCP. This indicates the substitution of hydrogen phosphate ions by carboxylate ions.[46] The FT-IR spectra (Figure 6b) of the sample synthesized at 40 °C revealed the absence of an absorption peak at 1193 cm^{-1}, and the bands ranging from 1400 to 1650 cm^{-1} are derived from carboxylate groups.[48] This unique observation could be linked to the stability of the carboxylate ion at 40 °C. Higher temperature might lead to decarboxylation. Therefore, conducting additional experiments is necessary to substantiate this hypothesis. It has been reported that the asymmetric stretch of the carboxylate ion is found between 1540 and 1650 cm^{-1}, whereas the symmetric stretch is noticed between 1360 and 1450 cm^{-1}. The asymmetric stretch is more intense than the symmetric stretch. Both bands must coexist in the FT-IR spectra to confirm the existence of carboxylate in a sample.[50,51] The absorption bands ranging from 1424 to 1457 and 1572 to 1650 cm^{-1} would be derived from the carboxylate ion present in OCP. The bending OH vibration was found to be masked with the absorption peaks derived from the carboxylate group at 1644 cm^{-1}.[52] This analysis confirms the existence of functional groups related to both the OCP and carboxylate. Moreover, a recent article describing the governing role of the carboxylate moiety in the mineralization of interfibrillar collagen indicated that only the hydrated layer of CaP has potential to incorporate carboxylate ions.[53] The association of the OCP with carboxylate (acetate) is a complex process, and more advanced analysis is required to depict the exact interaction.

3.2.3. SEM Analysis. The surface morphology of the synthesized samples (Figure 7) was found to have a plate-like structure, which is the characteristic morphology of the OCP. The synthesis temperature highly influenced the plate-like structure of the samples. It can be seen from the SEM images that the length of platted structures increased with the increase in temperature. Thus, the formation of larger particles at higher temperature is presumed due to either crystal growth or fusion of particles. Previously, it has been found that the

https://doi.org/10.1021/acsomega.4c01436
ACS Omega 2024, 9, 36165−36176

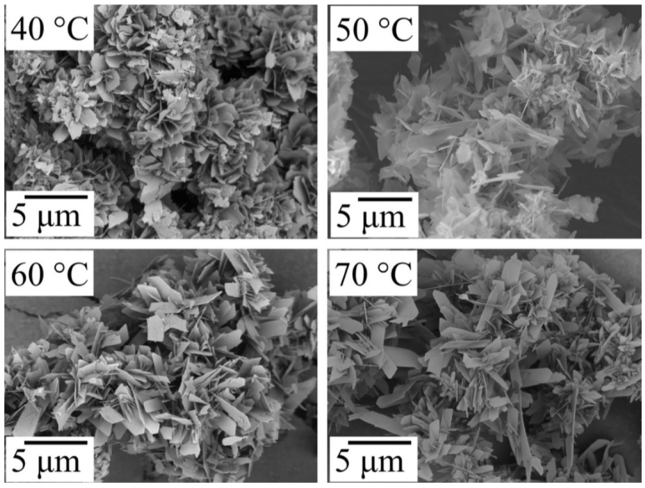

Figure 7. SEM micrographs of samples prepared at different temperatures.

growth of crystals is directly proportional to temperature.[54] This observation indicates that the temperature alters the morphological architecture of the OCP. A previous study reported a similar observation during the aging process of OCP samples.[21]

3.3. Effect of Synthesis Time. *3.3.1. XRD Analysis.* The influence of the synthesis time (calcium addition duration) on the formation of the OCP was studied at pH 6. Figure 8 shows the XRD pattern of the samples prepared in different synthesis durations (30, 60, and 120 min) without aging the reaction mixture. All the samples exhibited the presence of the OCP phase, which matched the standard ICDD pattern 00-026-1056. The XRD pattern revealed the existence of (100), (200), and (010) reflection peaks associated with OCP at 4.7° 2θ, 9.4° 2θ, and 9.7° 2θ. As the reaction temperature (from 40 to 70 °C) and time (from 30 to 120 min) were increased, the diffraction peaks also intensified. This is an indication that the reaction temperature as well as time influences the crystallite size of OCP samples. The long-term stability of the synthesized samples after 1 year of storage was studied and discussed in the Supporting Information (Figure S4).

3.3.2. FT-IR Analysis. FT-IR analysis (Figure 9) of the samples synthesized at different reaction times revealed the existence of different functional groups associated with the OCP as discussed in subsection Section 2.2.2 (Figure 6a). Additional information in the form of Supporting Information (Figure S3) has been included to illustrate the impact of various reaction times (ranging from 15 to 120 min) while maintaining a constant temperature of 30 °C and pH of 6.

3.3.3. SEM Analysis. The scanning electron micrographs of the samples prepared at different synthesis temperatures and times are shown in Figure 10. The samples revealed that the particles exhibit plate-like structures scattered throughout the surface. The most distinguishing feature observed among all samples was the increase in the length of the plate-like particles. Thus, the increase in the synthesis time (from 30 min to 2 h) resulted in the formation of longer ribbon-shaped particles. An earlier study reported that longer aging periods (3 and 12 h) resulted in an increase in the length of OCP particles,[21] whereas in the current study, the short plate-like architecture of the OCP particles grew into a belt-like structure with the increase in temperature and time.

The structure of the OCP is composed of an apatite layer and a hydrated layer arranged alternatively after each other, perpendicular to the *a* direction. The calcium and phosphate ions are arranged in the apatite layer like in the case of hydroxyapatite, whereas the hydrated layer comprises hydrogen phosphate, hydroxyl ions, and water (H_2O). The accumulation of ions (Ca^{2+} and PO_4^{3-}) from the mother solution on the (100) plane leads to the crystal growth of OCP. The affinity of these ions, specifically toward the (100) face of the apatite layer, is higher than that toward the other faces because the crystal plane (100) is the highest energetic face of OCP in the presence of water.[55] The ions tend to lower the overall surface energy by apposition on the (100) face. This process leads to an increase in the height of (100) reflection as observed in the XRD patterns (Figures 4 and 8) due to the increase of the crystallite size in this direction as well as the formation of longer ribbon-shaped particles as evidenced in SEM images (Figure 10). Concerning the above

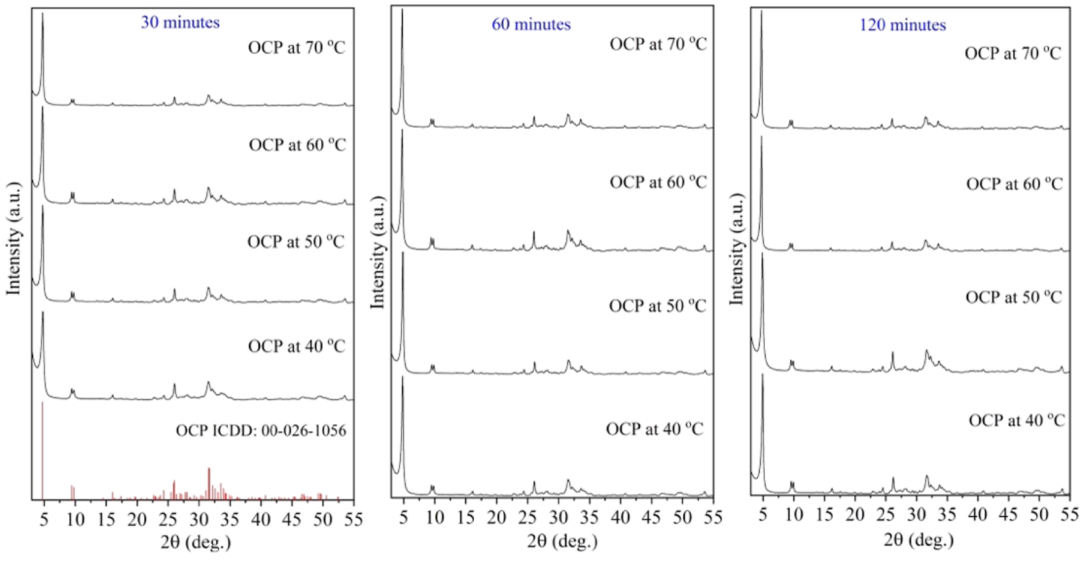

Figure 8. XRD patterns of the OCP samples prepared at different synthesis durations.

https://doi.org/10.1021/acsomega.4c01436
ACS Omega 2024, 9, 36165−36176

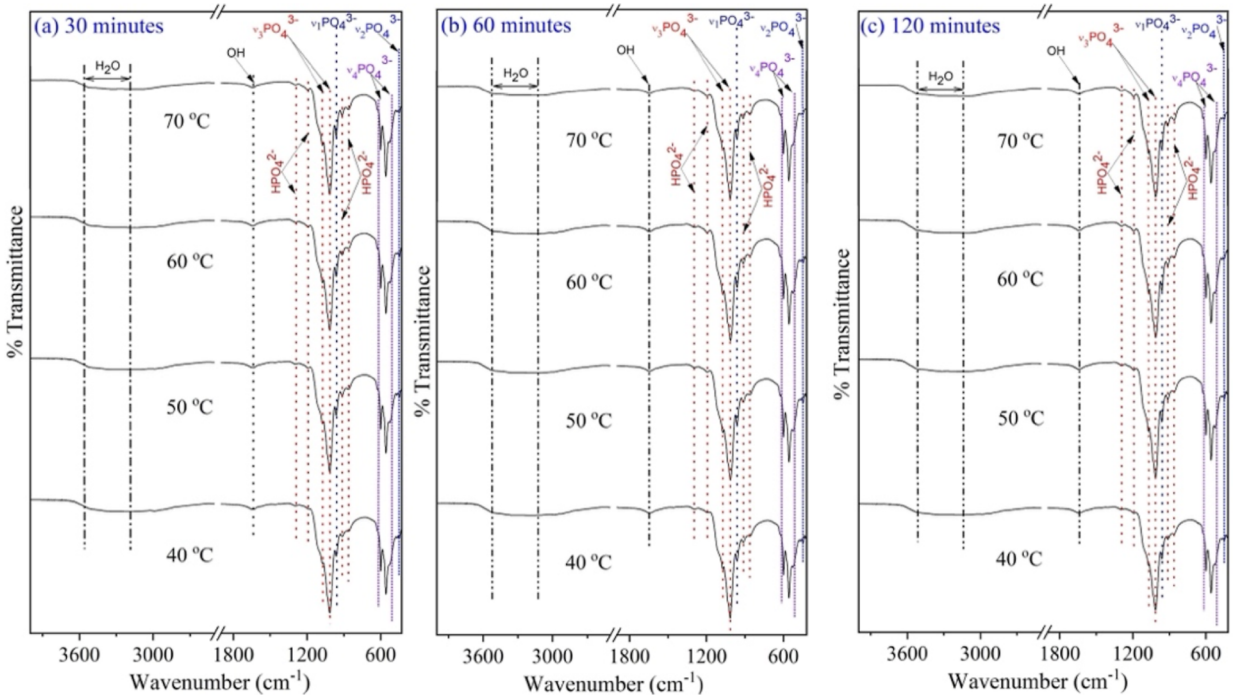

Figure 9. FT-IR spectra of OCP samples prepared in 30 (a), 60 (b), and 120 min (c).

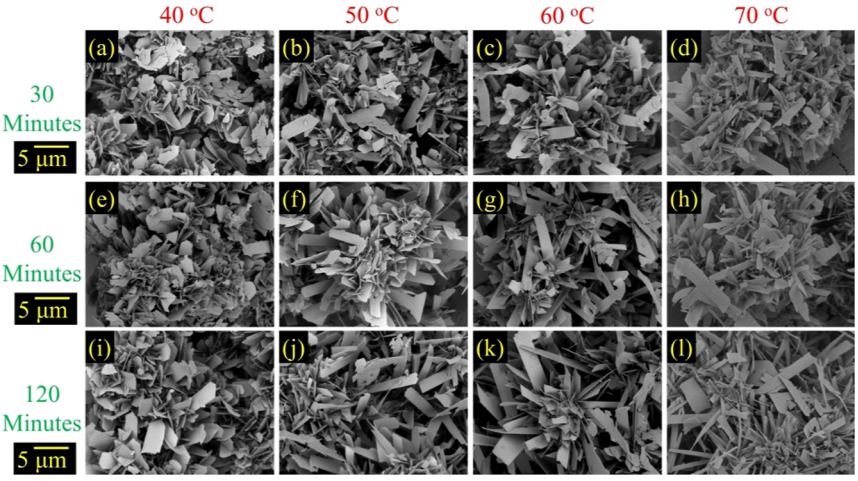

Figure 10. SEM images of OCP samples prepared at different synthesis temperatures in 30 (a–d), 60 (e–h), and 120 min (i–l).

discussion and the results observed in the present study, it can be suggested that an increase in reaction temperature (40 to 70 °C) and synthesis time (15 to 120 min) leads to elongation of OCP crystals visible under SEM and increases the crystallite size (*i.e.*, the size of the coherent scattering domains, determined by XRD analysis) along the *a* direction. An increase of the (100) peak height (or the OCP peaks in general) might further result from an increase of the quantity of crystalline OCP in the sample. Indeed, the Rietveld scale factors, which are proportional to the phase quantities, were around 40% higher in the 70 °C sample. Hence, it is possible that a more amorphous CaP phase is present in the 40 °C sample.

3.3.4. SSA Analysis. The SSA of the synthesized OCP samples (Figure 11) was studied by BET analysis. The SSA of the synthesized OCP samples (bar graph) is shown in the Supporting Information (Figure S5). The SSA of the OCP samples was highly influenced by the reaction temperature and time. The SSA of the samples followed a decreasing trend as the reaction temperature was raised from 40 to 70 °C and a similar trend was observed when the reaction time was increased from 15 to 120 min. Thus, the highest SSA (91 m^2/g) corresponds to the sample prepared at 40 °C in 15 min, which is 5 times higher than the sample produced in 120 min at 70 °C (16 m^2/g). Moreover, considering the reactions completed in 15 min, the SSA of the OCP produced at 40 °C is 3 times higher than that of the samples prepared at 60 and 70 °C, respectively.

The OCP samples prepared in 2 days exhibited different surface areas such as 1.2, 4.62, 26, and 62 m^2/g.[14] In a recent article, OCP synthesized using the hydrolysis method over a 3 day period exhibited an SSA of 66 m^2/g.[18] Compared to previous findings, the present study reports the highest known SSA of the OCP (91 m^2/g synthesized within 15 min). Thus, the methodology developed in the present work has the potential to synthesize tailor-made OCP with different SSA.

https://doi.org/10.1021/acsomega.4c01436
ACS Omega 2024, 9, 36165−36176

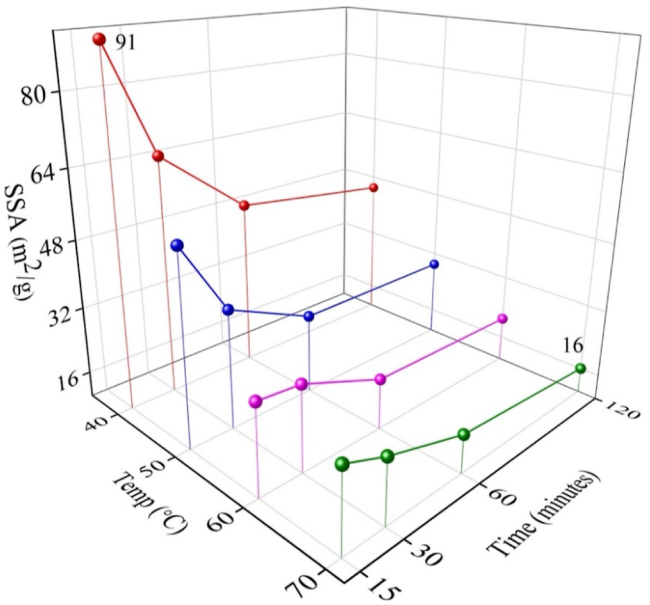

Figure 11. SSA of OCP samples prepared at different temperatures and synthesis durations.

The high SSA biomaterials offer enhanced reactivity, increased adsorption capacity, and improved efficiency across various processes and technologies. They play a pivotal role in facilitating the adsorption of bioactive molecules, including proteins and cytokines, onto biomaterial surfaces, thereby accelerating biomaterial integration and tissue regeneration.[56] SSA also governs a material's drug adsorption capability, making it a valuable parameter for drug adsorption.[57] For instance, the comparison of risedronate adsorption between HAp and zinc-substituted hydroxyapatite (ZnHA) demonstrated that ZnHA's larger surface area (86 m^2/g) resulted in superior risedronate adsorption compared to HAp (23 m^2/g).[58] Furthermore, the commercial success of deproteinized bovine bone mineral, with a high SSA of up to 88 m^2/g,[59] comparable to that of natural bone (ranging from 40 to 240 m^2/g),[60] underscores the growing demand for high SSA biomaterials in biomedical applications.

3.3.5. Particle Size Analysis. The particle size distribution of the OCP sample used for cellular studies is shown in Figure 12. Both the samples revealed monomodal curves. The average particle size of the sample synthesized at 40 °C was found to be 13 μm, whereas in the case of 70 °C, it was found to be 27 μm (Table 3).

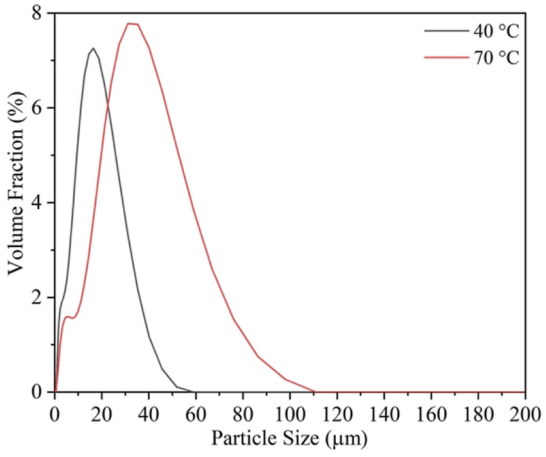

Figure 12. Particle size distribution of the OCP samples.

Table 3. Particle Size of Synthesized OCP Samples

S. no.	OCP samples	d0.5 (μm)
1	40 °C in 15 min	13 ± 0.1
2	70 °C in 120 min	27 ± 0.5

3.4. Cellular Studies. The impact of OCP synthesis temperature and resulting changes in SSA and particle size on cell viability was explored (Figure 13). The study, conducted in line with ISO 10993-5:2009 guidelines, demonstrated that none of the tested OCP extracts or their dilutions exhibited cytotoxic effects, with all experiments consistently revealing cell viability exceeding 70%. In most of the experiments, dilutions exhibited no significant differences when compared to extracts. Nonetheless, statistical analysis revealed the presence of statistically significant differences ($*p < 0.05$) in select cases. A decrease in cell viability was noted for OCP extracts with lower SSA following a 48 h incubation period. In previous studies, the suppressive influence of OCP on the proliferation of osteoblastic cells was similarly noted;[61] however, in prolonged incubation, proliferation of ST-2 cells was similar to cells grown on HAp or β-tricalcium phosphate—clinically already used materials.[62] Kovrlija *et al.* recently demonstrated that CaPs with dimensions comparable to cells (diameter 15–30 μm) could generate false events in vitro analysis.[63] Furthermore, investigation of hydroxyapatite particle size and shape influence on inflammatory responses revealed that particles in the mean size of 5 μm induce higher IL-1β secretion compared to larger particles (mean size 20 and 100 μm).[64] Therefore, our study also highlights the impact of particle size in *in vitro* analysis. Another major factor involved in the cell viability is the dissolution process of the OCP through its hydrolysis to calcium-deficient hydroxyapatite. The

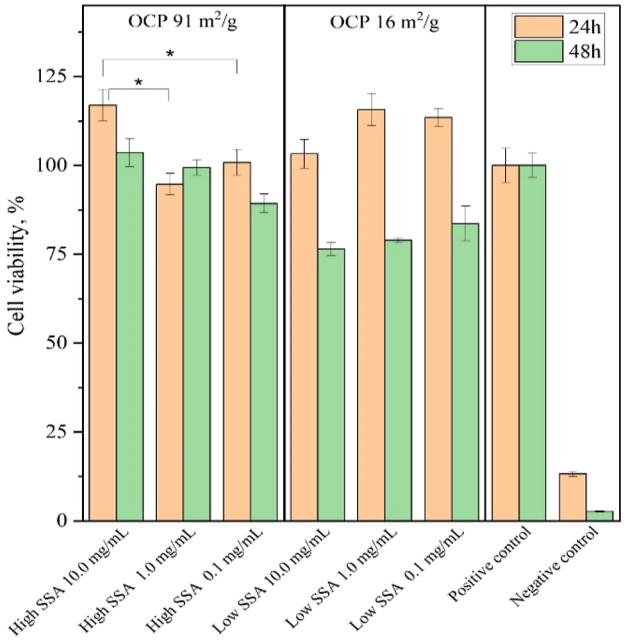

Figure 13. Effect of OCP sample extracts on MC3T3-E1 cell viability.

https://doi.org/10.1021/acsomega.4c01436
ACS Omega 2024, 9, 36165−36176

OCP dissolution effect on the cellular viability has been studied extensively by Suzuki *et al.*[65] and Petrakova *et al.*[66] According to their studies, higher dissolution capacity ensures enhanced progressive Ca^{2+} ion incorporation in the OCP and inorganic phosphate ion release in the physiological environment. Also, nonlinear calcium ion adsorption from the cell culture medium decreases the proliferation rate for bone cell lines and formation of calcium-deficient hydroxyapatite provokes acidification of culture media,[67] therefore we see the decrease of the cell viability in the 48 h time point.

4. CONCLUSIONS

Current research reports an ultrafast and straightforward procedure for the synthesis of OCP within minutes. The phase formation of the OCP was found to be influenced by pH, temperature, and order of reagent addition. The presence of brushite and HAp phases was noticed at pH lower and higher than 6. Even if the pH is controlled at 6, a temperature of 40 to 70 °C is necessary for the formation of the OCP. The length of the plate-like structure of the OCP particles increased with the increase in reaction temperature and time. The processing schemes enabled the synthesis of OCP with varying SSAs. The SSA of the OCP samples can be tuned as desired by altering the reaction temperature and time. The highest SSA sample revealed a higher cell viability than the lowest SSA sample. This research was focused on developing a protocol for the facile synthesis of the OCP, but surprisingly, the possible formation of OCPC was also encountered at 40 °C. The present work suggests that the high SSA OCP samples can be explored as scaffolds, composites for hard tissue regeneration, or carriers of therapeutic molecules for drug delivery applications.

■ ASSOCIATED CONTENT

Data Availability Statement

Data will be made available on request. We can upload the XRD raw data and BET data in Zenodo after publishing.

Supporting Information

The Supporting Information is available free of charge at https://pubs.acs.org/doi/10.1021/acsomega.4c01436.

Effect of pH (image of the pH profile of samples and FT-IR spectra of samples prepared at different pHs), effect of the order of reagent addition (XRD pattern), effect of reaction temperature (XRD pattern and FT-IR spectra), stability study of OCP samples after 1 year of storage (XRD analysis), image of the SSA of synthesized OCP, and table containing the SSA values of OCP as reported in the literature (PDF)

■ AUTHOR INFORMATION

Corresponding Authors

Rajan Choudhary − *School of Chemistry, University College Dublin, Belfield Dublin 4, Ireland; Institute of Biomaterials and Bioengineering, Faculty of Natural Sciences and Technology, Riga Technical University, Riga LV-1007, Latvia; Baltic Biomaterials Centre of Excellence, Headquarters at Riga Technical University, Riga LV-1048, Latvia*; Email: rajan.choudhary@ucd.ie

Janis Locs − *Institute of Biomaterials and Bioengineering, Faculty of Natural Sciences and Technology, Riga Technical University, Riga LV-1007, Latvia; Baltic Biomaterials Centre of Excellence, Headquarters at Riga Technical University, Riga LV-1048, Latvia*; orcid.org/0000-0003-3162-7431; Email: janis.locs@rtu.lv

Authors

Abhishek Indurkar − *Institute of Biomaterials and Bioengineering, Faculty of Natural Sciences and Technology, Riga Technical University, Riga LV-1007, Latvia; Baltic Biomaterials Centre of Excellence, Headquarters at Riga Technical University, Riga LV-1048, Latvia*; orcid.org/0000-0002-3971-9077

Kristaps Rubenis − *Institute of Biomaterials and Bioengineering, Faculty of Natural Sciences and Technology, Riga Technical University, Riga LV-1007, Latvia; Baltic Biomaterials Centre of Excellence, Headquarters at Riga Technical University, Riga LV-1048, Latvia*; orcid.org/0000-0002-9044-8479

Andra Grava − *Institute of Biomaterials and Bioengineering, Faculty of Natural Sciences and Technology, Riga Technical University, Riga LV-1007, Latvia; Baltic Biomaterials Centre of Excellence, Headquarters at Riga Technical University, Riga LV-1048, Latvia*

Arita Dubnika − *Institute of Biomaterials and Bioengineering, Faculty of Natural Sciences and Technology, Riga Technical University, Riga LV-1007, Latvia; Baltic Biomaterials Centre of Excellence, Headquarters at Riga Technical University, Riga LV-1048, Latvia*

Katrin Hurle − *GeoZentrum Nordbayern, Mineralogy, Friedrich-Alexander-Universität Erlangen-Nuernberg (FAU), Erlangen 91054, Germany*; orcid.org/0000-0003-0494-6795

Complete contact information is available at: https://pubs.acs.org/10.1021/acsomega.4c01436

Notes

The authors declare no competing financial interest.

■ ACKNOWLEDGMENTS

The authors acknowledge financial support from the European Union's Horizon 2020 research and innovation programme under the grant agreement no. 857287 (BBCE—Baltic Biomaterials Centre of Excellence).

■ REFERENCES

(1) Suzuki, O.; Shiwaku, Y.; Hamai, R. Octacalcium Phosphate Bone Substitute Materials: Comparison between Properties of Biomaterials and Other Calcium Phosphate Materials. *Dent. Mater. J.* **2020**, *39*, 187−199.

(2) Kovrlija, I.; Locs, J.; Loca, D. Octacalcium Phosphate: Innovative Vehicle for the Local Biologically Active Substance Delivery in Bone Regeneration. *Acta Biomater.* **2021**, *135*, 27−47.

(3) Murray, K. A.; Döbelin, N.; Albadarin, A. B.; Sadło, J.; Ren, G.; Collins, M. N.; O'Neill, C. The influence of sterilization on octacalcium phosphate for clinical applications. In *Octacalcium Phosphate Biomaterials: Understanding of Bioactive Properties and Application*; Insley, G., Suzuki, O., Eds.; Woodhead Publishing, 2020; pp 55−84.

(4) Brown, W. E.; Lehr, J. R.; Smith, J. P.; Frazier, A. W. Crystallography of octacalcium phosphate. *J. Am. Chem. Soc.* **1957**, *79*, 5318−5319.

(5) Brown, W. E. Octacalcium phosphate and hydroxyapatite: Crystal structure of octacalcium phosphate. *Nature* **1962**, *196*, 1048−1050.

(6) Indurkar, A.; Choudhary, R.; Rubenis, K.; Locs, J. Advances in Sintering Techniques for Calcium Phosphates Ceramics. *Materials* **2021**, *14*, 6133.

(7) Rey, C.; Combes, C. What Bridges Mineral Platelets of Bone? *BoneKEy Rep.* **2014**, *3*, 586.
(8) Suzuki, O.; Imaizumi, H.; Kamakura, S.; Katagiri, T. Bone Regeneration by Synthetic Octacalcium Phosphate and its Role in Biological Mineralization. *Curr. Med. Chem.* **2008**, *15*, 305−313.
(9) Komlev, V. S.; Bozo, I. I.; Deev, R. V.; Gurin, A. N. Bioactivity and effect of bone formation for octacalcium phosphate ceramics. In *Octacalcium Phosphate Biomaterials: Understanding of Bioactive Properties and Application*; Insley, G., Suzuki, O., Eds.; Woodhead Publishing, 2020; pp 85−119.
(10) Sheikh, Z.; Najeeb, S.; Khurshid, Z.; Verma, V.; Rashid, H.; Glogauer, M. Biodegradable Materials for Bone Repair and Tissue Engineering Applications. *Materials* **2015**, *8*, 5744−5794.
(11) Kamakura, S.; Sasano, Y.; Homma, H.; Suzuki, O.; Kagayama, M.; Motegi, K. Implantation of Octacalcium Phosphate (OCP) in Rat Skull Defects Enhances Bone Repair. *J. Dent. Res.* **1999**, *78*, 1682−1687.
(12) Kim, J.; Kim, S.; Song, I. Biomimetic octacalcium phosphate bone has superior bone regeneration ability compared to xenogeneic or synthetic bone. *Materials* **2021**, *14*, 5300.
(13) Kikawa, T.; Kashimoto, O.; Imaizumi, H.; Kokubun, S.; Suzuki, O. Intramembranous Bone Tissue Response to Biodegradable Octacalcium Phosphate Implant. *Acta Biomater.* **2009**, *5*, 1756−1766.
(14) Shelton, R. M.; Liu, Y.; Cooper, P. R.; Gbureck, U.; German, M. J.; Barralet, J. E. Bone Marrow Cell Gene Expression and Tissue Construct Assembly Using Octacalcium Phosphate Microscaffolds. *Biomaterials* **2006**, *27*, 2874−2881.
(15) Barinov, S. M.; Komlev, V. S. Osteoinductive Ceramic Materials for Bone Tissue Restoration: Octacalcium Phosphate (Review). *Inorg. Mater. Appl. Res.* **2010**, *1*, 175−181.
(16) O'Sullivan, R.; Kelly, D. Synthesis methodologies options for large-scale manufacturer of octacalcium phosphate. In *Octacalcium Phosphate Biomaterials: Understanding of Bioactive Properties and Application*; Insley, G., Suzuki, O., Eds.; Woodhead Publishing, 2020; pp 147−176.
(17) Rey, C. C.; Combes, C.; Drouet, C. Synthesis and physical chemical characterizations of octacalcium phosphate-based biomaterials for hard-tissue regeneration. In *Octacalcium Phosphate Biomaterials: Understanding of Bioactive Properties and Application*; Insley, G., Suzuki, O., Eds.; Woodhead Publishing, 2020; pp 177−212.
(18) Kovrlija, I.; Menshikh, K.; Marsan, O.; Rey, C.; Combes, C.; Locs, J.; Loca, D. Exploring the Formation Kinetics of Octacalcium Phosphate from Alpha-Tricalcium Phosphate: Synthesis Scale-Up, Determination of Transient Phases, Their Morphology and Biocompatibility. *Biomolecules* **2023**, *13*, 462.
(19) LeGeros, R. Z. Preparation of octacalcium phosphate (OCP): A direct fast method. *Calcif. Tissue Int.* **1985**, *37*, 194−197.
(20) Suzuki, O.; Nakamura, M.; Miyasaka, Y.; Kagayama, M.; Sakurai, M. Bone Formation on Synthetic Precursors of Hydroxyapatite. *Tohoku J. Exp. Med.* **1991**, *164*, 37−50.
(21) Saengdet, P.; Ogawa, M. Directional growth of octacalcium phosphate using micro-flow reactor mixing and subsequent aging. *RSC Adv.* **2021**, *11*, 15969−15976.
(22) Graham, S.; Brown, P. W. The low temperature formation of octacalcium phosphate. *J. Cryst. Growth* **1993**, *132*, 215−225.
(23) Bigi, A.; Boanini, E.; Borghi, M.; Cojazzi, G.; Panzavolta, S.; Roveri, N. Synthesis and hydrolysis of octacalcium phosphate: Effect of sodium polyacrylate. *J. Inorg. Biochem.* **1999**, *75*, 145−151.
(24) Arellano-Jiménez, M.; García-García, R.; Reyes-Gasga, J. Synthesis and hydrolysis of octacalcium phosphate and its characterization by electron microscopy and X-ray diffraction. *J. Phys. Chem. Solids* **2009**, *70*, 390−395.
(25) Bigi, A.; Boanini, E.; Walsh, D.; Mann, S. Morphosynthesis of Octacalcium Phosphate Hollow Microspheres by Polyelectrolyte-Mediated Crystallization This work was supported by MURST, the University of Bologna (Funds for Selected Research Topics), and the EPSRC (UK). *Angew. Chem., Int. Ed.* **2002**, *41*, 2163.
(26) Forte, L.; Torricelli, P.; Boanini, E.; Gazzano, M.; Fini, M.; Bigi, A. Antiresorptive and anti-angiogenetic octacalcium phosphate functionalized with bisphosphonates: An in vitro tri-culture study. *Acta Biomater.* **2017**, *54*, 419−428.
(27) Bigi, A.; Bracci, B.; Panzavolta, S.; Iliescu, M.; Plouet-Richard, M.; Werckmann, J.; Cam, D. Morphological and Structural Modifications of Octacalcium Phosphate Induced by Poly-l-Aspartate. *Cryst. Growth Des.* **2004**, *4*, 141−146.
(28) Temizel, N.; Girisken, G.; Tas, A. C. Accelerated transformation of brushite to octacalcium phosphate in new biomineralization media between 36.5°C and 80°C. *Mater. Sci. Eng.: C* **2011**, *31*, 1136−1143.
(29) Heydari, Z.; Mohebbi-Kalhori, D.; Afarani, M. S. Engineered Electrospun Polycaprolactone (PCL)/Octacalcium Phosphate (OCP) Scaffold for Bone Tissue Engineering. *Mater. Sci. Eng.: C* **2017**, *81*, 127−132.
(30) Sugiura, Y.; Munar, M. L.; Ishikawa, K. Fabrication of Octacalcium Phosphate Foam through Phase Conversion and Its Histological Evaluation. *Mater. Lett.* **2018**, *212*, 28−31.
(31) Sugiura, Y.; Ishikawa, K. Effect of Calcium and Phosphate on Compositional Conversion from Dicalcium Hydrogen Phosphate Dihydrate Blocks to Octacalcium Phosphate Blocks. *Crystals* **2018**, *8*, 222.
(32) Sugiura, Y.; Ishikawa, K. Fabrication of Pure Octacalcium Phosphate Blocks from Dicalcium Hydrogen Phosphate Dihydrate Blocks via a Dissolution-Precipitation Reaction in a Basic Solution. *Mater. Lett.* **2019**, *239*, 143−146.
(33) Sugiura, Y.; Munar, M. L.; Ishikawa, K. Fabrication of Octacalcium Phosphate Block through a Dissolution-Precipitation Reaction Using a Calcium Sulphate Hemihydrate Block as a Precursor. *J. Mater. Sci.: Mater. Med.* **2018**, *29*, 151.
(34) Tripathi, G.; Miyazaki, T. Spontaneous Fabrication of Octacalcium Phosphate: Synthesis Conditions and Basic Characterizations. *Bull. Mater. Sci.* **2021**, *44*, 163.
(35) Teterina, A. Yu.; Smirnov, I. V.; Fadeeva, I. S.; Fadeev, R. S.; Smirnova, P. V.; Minaychev, V. V.; Kobyakova, M. I.; Fedotov, A. Yu.; Barinov, S. M.; Komlev, V. S. Octacalcium Phosphate for Bone Tissue Engineering: Synthesis, Modification, and In Vitro Biocompatibility Assessment. *Int. J. Mol. Sci.* **2021**, *22*, 12747.
(36) Mathew, M.; Brown, W. E.; Schroeder, L. W.; Dickens, B. Crystal structure of octacalcium bis(hydrogenphosphate) tetrakis(phosphate)pentahydrate, $Ca_8(HP0_4)_2(PO_4)_4{\cdot}5H_2O$. *J. Crystallogr. Spectrosc. Res.* **1988**, *18*, 235−250.
(37) Ectors, D.; Goetz-Neunhoeffer, F.; Neubauer, J. A Generalized Geometric Approach to Anisotropic Peak Broadening Due to Domain Morphology. *J. Appl. Crystallogr.* **2015**, *48*, 189−194.
(38) Sudarsanan, K.; Young, R. A. Significant Precision in Crystal Structural Details. Holly Springs Hydroxyapatite. *Acta Crystallogr. B Struct. Crystallogr. Cryst. Chem.* **1969**, *25*, 1534−1543.
(39) Reynaud, C.; Thomas, C.; Casale, S.; Nowak, S.; Costentin, G. Development of a Thermodynamic Approach to Assist the Control of the Precipitation of Hydroxyapatites and Associated Calcium Phosphates in Open Systems. *CrystEngComm* **2021**, *23*, 4857−4870.
(40) Gagliardi, L. G.; Tascon, M.; Castells, C. B. Effect of Temperature on Acid-Base Equilibria in Separation Techniques. A Review. *Anal. Chim. Acta* **2015**, *889*, 35−57.
(41) Kamitakahara, M.; Okano, H.; Tanihara, M.; Ohtsuki, C. Synthesis of Octacalcium Phosphate Intercalated with Dicarboxylate Ions from Calcium Carbonate and Phosphoric Acid. *J. Ceram. Soc. Japan* **2008**, *116*, 481−485.
(42) Komlev, V. S.; Fadeeva, I. V.; Fomin, A. S.; Shvorneva, L. I.; Ferro, D.; Barinov, S. M. Synthesis of Octacalcium Phosphate by Precipitation from Solution. *Dokl. Chem.* **2010**, *432*, 178−182.
(43) Wiesner, A. D.; Katz, L. E.; Chen, C.-C. The Impact of Ionic Strength and Background Electrolyte on pH Measurements in Metal Ion Adsorption Experiments. *J. Colloid Interface Sci.* **2006**, *301*, 329−332.
(44) Nancollas, G. H.; Zhang, J. Formation and Dissolution Mechanisms of Calcium Phosphates in Aqueous Systems. In *In Hydroxyapatite and Related Materials*; Brown, P. W., Constantz, B., Eds.; CRC Press, 2017; pp 73−81.

https://doi.org/10.1021/acsomega.4c01436
ACS Omega 2024, 9, 36165−36176

(45) Yokoi, T.; Shimabukuro, M.; Kawashita, M. Octacalcium Phosphate with Incorporated Carboxylate Ions: A Review. *Sci. Technol. Adv. Mater.* **2022**, *23*, 434−445.
(46) Yokoi, T.; Watanabe, M.; Goto, T.; Meng, S.; Sekino, T.; Shimabukuro, M.; Kawashita, M. Synthesis of Octacalcium Phosphate Containing Glutarate Ions with a High Incorporation Fraction. *Materials* **2023**, *16*, 64.
(47) Davies, E.; Müller, K. H.; Wong, W. C.; Pickard, C. J.; Reid, D. G.; Skepper, J. N.; Duer, M. J. Citrate Bridges between Mineral Platelets in Bone. *Proc. Natl. Acad. Sci. U.S.A.* **2014**, *111*, E1354−E1363.
(48) Monma, H.; Goto, M. Succinate-Complexed Octacalcium Phosphate. *Bull. Chem. Soc. Jpn.* **1983**, *56*, 3843−3844.
(49) Fowler, B. O.; Markovic, M.; Brown, W. E. Octacalcium phosphate. 3. Infrared and Raman vibrational spectra. *3. Infrared and Raman Vibrational Spectra. Chem. Mater.* **1993**, *5*, 1417−1423.
(50) Smith, B. *Infrared Spectral Interpretation: a Systematic Approach*, 1st ed.; CRC Press: Boca Raton, 1998.
(51) Yokoi, T.; Goto, T.; Hara, M.; Sekino, T.; Seki, T.; Kamitakahara, M.; Ohtsuki, C.; Kitaoka, S.; Takahashi, S.; Kawashita, M. Incorporation of Tetracarboxylate Ions into Octacalcium Phosphate for the Development of Next-Generation Biofriendly Materials. *Commun. Chem.* **2021**, *4*, 4.
(52) Kukueva, E. V.; Putlyaev, V. I.; Tikhonov, A. A.; Safronova, T. V. Octacalcium Phosphate as a Precursor for the Fabrication of Composite Bioceramics. *Inorg. Mater.* **2017**, *53*, 212−219.
(53) Indurkar, A.; Choudhary, R.; Rubenis, K.; Locs, J. Role of Carboxylic Organic Molecules in Interfibrillar Collagen Mineralization. *Front. Bioeng. Biotechnol.* **2023**, *11*, 1150037.
(54) Myerson, A. S.; Erdemir, D.; Lee, A. Y. *Handbook of Industrial Crystallization*, 3rd ed.; Cambridge University Press, 2019.
(55) Zhao, W.; Xu, Z.; Yang, Y.; Sahai, N. Surface Energetics of the Hydroxyapatite Nanocrystal-Water Interface: A Molecular Dynamics Study. *Langmuir* **2014**, *30*, 13283−13292.
(56) Xiao, D.; Zhang, J.; Zhang, C.; Barbieri, D.; Yuan, H.; Moroni, L.; Feng, G. The Role of Calcium Phosphate Surface Structure in Osteogenesis and the Mechanisms Involved. *Acta Biomater.* **2020**, *106*, 22−33.
(57) Wen, Y.; Li, J.; Lin, H.; Huang, H.; Song, K.; Duan, K.; Guo, T.; Weng, J. Improvement of Drug-Loading Properties of Hydroxyapatite Particles Using Triethylamine as a Capping Agent: A Novel Approach. *Crystals* **2021**, *11*, 703.
(58) Forte, L.; Sarda, S.; Combes, C.; Brouillet, F.; Gazzano, M.; Marsan, O.; Boanini, E.; Bigi, A. Hydroxyapatite functionalization to trigger adsorption and release of risedronate. *B Biointerfaces.* **2017**, *160*, 493−499.
(59) Lee, D. S. H.; Pai, Y.; Chang, S. Physicochemical characterization of InterOss® and Bio-Oss® anorganic bovine bone grafting material for oral surgery − A comparative study. *Mater. Chem. Phys.* **2014**, *146*, 99−104.
(60) Kolmas, J.; Ślósarczyk, A.; Wojtowicz, A.; Kolodziejski, W. Estimation of the Specific Surface Area of Apatites in Human Mineralized Tissues Using 31P MAS NMR. *Solid State Nucl. Magn. Reason.* **2007**, *32*, 53−58.
(61) Suzuki, O.; Kamakura, S.; Katagiri, T. Surface Chemistry and Biological Responses to Synthetic Octacalcium Phosphate. *J. Biomed. Mater. Res.* **2006**, *77B*, 201−212.
(62) Morimoto, S.; Anada, T.; Honda, Y.; Suzuki, O. Comparative Study on *in Vitro* Biocompatibility of Synthetic Octacalcium Phosphate and Calcium Phosphate Ceramics Used Clinically. *Biomed. Mater.* **2012**, *7*, 045020.
(63) Kovrlija, I.; Menshikh, K.; Abreu, H.; Cochis, A.; Rimondini, L.; Marsan, O.; Rey, C.; Combes, C.; Locs, J.; Loca, D. Challenging Applicability of ISO 10993−5 for Calcium Phosphate Biomaterials Evaluation: Towards More Accurate in Vitro Cytotoxicity Assessment. *Biomater. Adv.* **2024**, *160*, 213866.
(64) Lebre, F.; Sridharan, R.; Sawkins, M. J.; Kelly, D. J.; O'Brien, F. J.; Lavelle, E. C. The Shape and Size of Hydroxyapatite Particles Dictate Inflammatory Responses Following Implantation. *Sci. Rep.* **2017**, *7* (1), 2922.
(65) Suzuki, O.; Hamai, R.; Sakai, S. Corrigendum to "The material design of octacalcium phosphate bone substitute: increased dissolution and osteogenecity". Volume 158, 1 March 2023, Pages 1-11. *Acta Biomater.* **2023**, *161*, 325.
(66) Petrakova, N. V.; Teterina, A. Yu.; Mikheeva, P. V.; Akhmedova, S. A.; Kuvshinova, E. A.; Sviridova, I. K.; Sergeeva, N. S.; Smirnov, I. V.; Fedotov, A. Yu.; Kargin, Y. F.; Barinov, S. M.; Komlev, V. S. In Vitro Study of Octacalcium Phosphate Behavior in Different Model Solutions. *ACS Omega* **2021**, *6* (11), 7487−7498.
(67) Gustavsson, J.; Ginebra, M. P.; Engel, E.; Planell, J. Ion Reactivity of Calcium-Deficient Hydroxyapatite in Standard Cell Culture Media. *Acta Biomater.* **2011**, *7* (12), 4242−4252.

https://doi.org/10.1021/acsomega.4c01436
ACS Omega 2024, 9, 36165−36176